ARTICLE

Magnetic Epoxy Resin Nanocomposites Reinforced with Core–Shell Structured Fe@FeO Nanoparticles: Fabrication and Property Analysis

Jiahua Zhu,[†] Suying Wei,[‡] Jongeun Ryu,[§] Luyi Sun,[∥] Zhiping Luo,[⊥] and Zhanhu Guo*[,†]

Integrated Composites Laboratory (ICL), Dan F Smith Department of Chemical Engineering, and Department of Chemistry and Physics, Lamar University, Beaumont, Texas 77710, Department of Mechanical & Aerospace Engineering, University of California Los Angeles, Los Angeles, California 90095, Department of Chemistry and Biochemistry, Texas State University–San Marcos, San Marcos, Texas 78666, and Microscopy and Imaging Center, Texas A&M University, College Station, Texas 77843

ABSTRACT Epoxy resin nanocomposites reinforced with various loadings of core–shell structured nanoparticles (Fe@FeO) are prepared using a surface wetting method. Nanoparticle loading effect on the viscosity of epoxy monomers is well-correlated to Cross' rheological model. Dynamic mechanical analysis (DMA) results reveal that the glass transition temperature is increased by 10 °C with the addition of nanoparticles, which is surprisingly independent of the particle loadings. The saturation magnetization (M_s) of the 20 wt % Fe@FeO/epoxy nanocomposites is 17.03 emu/g, which is about 15.8% of that of the pure nanoparticles. Meanwhile, the coercivity increases from 62.33 to 202.13 Oe after the nanoparticles are dispersed in the epoxy matrix. The electrical conductivity percolation is found to be around 5–10 wt %, where the resistance of the nanocomposites sharply decreases by 6 orders of magnitude. Thermal stability and tensile properties of the pristine epoxy and nanocomposites are also investigated in this work.

KEYWORDS: polymer–matrix composites • magnetic properties • rheology • nanoparticles • electrical properties • mechanical properties;

INTRODUCTION

Composite materials have been extensively studied for their wide applications in various fields, such as aerospace, electronics, sports facilities, and vehicles. Polymeric nanocomposites (PNCs) reinforced with nanoparticles have attracted much interest because of their cost-effective processability, lightweight and tunable physical properties, such as mechanical, magnetic, optical, electric, and electronic properties (1–7). With all these unparallel advantages, polymer nanocomposites have found extensive applications such as proton conducting membranes for fuel cells (8), microwave absorption (9, 10), clay-reinforced fire retardant composites (11, 12), chromatic sensors (13) and capacitors (14).

Magnetic nanoparticles with a size close to the single-domain are of great interest in different fields of chemistry and physics because of their unique magnetic properties, such as high coercivity and their active chemical catalytic properties inherent with their small size and high specific surface area (15). Until now, most of the reported works about magnetic nanocomposites have been based on metal oxide magnetic nanoparticles in various polymers, such as vinyl-ester resin (16), polyurethane (10), and polymethyl methacrylate (17, 18), because of the easy oxidation of the metallic magnetic (Fe, Ni, Co) nanoparticles. Recently, we have discovered a facile monomer stabilization method to fabricate iron/vinyl ester resin nanocomposites (19). However, it is still a challenge to conveniently use the metallic magnetic nanoparticles at the industrial level because of their highly easy oxidation and flammability in air. To solve this challenge, two approaches are normally conducted to achieve a stable nanoparticle usable system. One is to use surfactant or polymer to stabilize the nanoparticles in a colloidal suspension which reduces particle agglomeration (20), and the other one is to introduce a stable shell structure to protect the metallic magnetic nanoparticles from oxidation in harsh environments (21). In this project, the commercially available core metal nanoparticles coated with a thin oxide layer for stabilization are selectively used for research convenience and for potential large quantity of polymer nanocomposites fabrication facing the current polymer nanocomposites field.

Epoxy resin, as an advanced material, displays a series of interesting characteristics and has been widely used in areas ranging from microelectronics to aerospace (22, 23).

* Corresponding author. E-mail: zhanhu.guo@lamar.edu. Phone: (409) 880-7654. Fax: (409) 880-7283.
Received for review April 26, 2010 and accepted June 21, 2010
[†] Integrated Composites Laboratory (ICL), Department of Chemical Engineering, Lamar University.
[‡] Department of Chemistry and Physics, Lamar University.
[§] University of California Los Angeles.
[∥] Texas State University–San Marcos.
[⊥] Texas A&M University.
DOI: 10.1021/am100361h

Published on Web 07/01/2010

One of the most commonly used formulations of high-temperature cured epoxy is Bisphenol F diglycidyl ether (Epon 862) with curing agent DETDA. When Epon 862 is cross-linked with appropriate curing agents, superior mechanical, adhesive, and chemical resistance properties can be obtained (24, 25). The processing parameters are essentially important for fabricating high-performance nanocomposites, most of which can be obtained from the rheological properties of such materials. However, it is still a challenge to study the rheological properties of thermosetting polymers, even harder for the polymer nanocomposites. Not only the difficulties to obtain rheological properties of the pristine polymer after curing process, but also the influence of nanoparticles on the rheological properties of the polymer. Studying the rheological properties of epoxy nanocomposite solution suspended with nanoparticles is an effective way to investigate the nanoparticle effect on the rheological properties of polymer and thus provides the key information for the processing parameters of nanocomposites.

In this work, core−shell structured nanoparticles (Fe@FeO) are used to reinforce epoxy resin because of their relative resistance to oxidation in air. The mechanical properties of the nanocomposites are evaluated by both dynamic mechanical analysis (DMA) and tensile tests. The fracture microstructure of the nanocomposites and the cured pure epoxy are evaluated with a scanning electron microscope (SEM). TEM observation reveals a uniform distribution without obvious agglomeration in the epoxy resin matrix. The thermal stability of the nanocomposites is investigated with thermogravimetric analysis (TGA). Finally, magnetic properties and electrical conductivity of the prepared Fe@FeO/epoxy nanocomposites are reported.

EXPERIMENTAL METHODS AND CHARACTERIZATION

Materials. The epoxy resin used is Epon 862 (bisphenol F epoxy) and EpiCure curing agent W, which are purchased from Miller-Stephenson Chemical Company, Inc. Core−shell structured Fe(core)@FeO(shell) nanoparticles, with a particle size of 15−25 nm and oxide thickness of 0.5 nm, are provided by QuantumSphere, Inc. All the materials are used as received without any further treatment.

Preparation of Fe@FeO/Epoxy Resin Nanocomposites. The cured epoxy resin is prepared by mixing Epon 862 with EpiCure curing agent W under mechanical stirring (200 rpm) for 4 h in a 70 °C water bath, and degassing the mixture under ultrasonication at room temperature for 30 min. The weight ratio of Epon 862 and Epicure W is 100:26.5 as recommended by the company. After removing the bubbles, the mixture is transferred to silicon-rubber dog-bone molds and cured at 120 °C for 5 h. The cured material is then trimmed. Finally, the samples are machined and polished for DMA and tensile tests.

The Fe@FeO/epoxy nanocomposites with Fe@FeO nanoparticle loading of 1, 5, 10, and 20 wt % are prepared, respectively. Fe@FeO nanoparticles are accurately weighed according to different weight percentage and then Epoxy 862 is added, keeping the mixture overnight until the surface of nanoparticles is wetted completely. The mixture is then stirred at 400 rpm for 1 h at room temperature. After that, Epicure curing agent W is added and further mechanical mixed (200 rpm) for 4 h at a 70 °C water bath. The curing cycle of Fe@FeO/epoxy nanocomposites is the same as used in curing the pristine epoxy.

Rheology. The rheological behaviors of the polymer nanocomposites solutions are investigated with an AR 2000ex Rheometer (TA Instrumental Company) at shear rates ranging from 0.1 to 1200 rad/s at 25 °C. A series of measurements are performed in a cone-and-plate geometry with a diameter of 40 mm and a truncation of 64 μm.

Density and Mechanical Property. The density of the pure epoxy and nanocomposites is measured following the American Society for Testing and Materials (ASTM, 2008, standard D 792−08) standard. Dynamic mechanical analysis (DMA) tests are conducted using a TA Instruments AR 2000 at a fixed frequency of 1 Hz. The sample dimensions are 12 × 3 × 40 mm^3. The sample is tested with the temperature ranging from room temperature to 200 °C at atmosphere pressure and a heating rate of 2 °C/min. The mechanical properties of the fabricated nanocomposites are evaluated by tensile tests following the American Society for Testing and Materials (ASTM, 2002, standard D 412−98a) standard. A testing machine (Comten Industries, model 945KRC0300; Loading unit, PSB5000; Digit controller, DMC 026S) with C-Tap 3.0 software testing machine is used. The samples are prepared according to the standard procedures. Five to seven specimens per sample were tested. Specimens that fractured at some obvious fortuitous flaws or near a grip are discarded. A crosshead speed of 1.52 mm/min is used and strain (mm/mm) is calculated by dividing the crosshead displacement by the gage length.

Morphology. The morphology of the fracture surface is characterized with scanning electron microscope (SEM, JEOL field emission scanning electron microscope, JSM-6700F). The SEM specimens are prepared by sputter coating a thin gold layer approximately 3 nm thick. The particle distribution in the epoxy resin matrix is examined by a transmission electron microscope (TEM). The samples are microtomed into thin sections with a thickness of less than 100 nm and then observed in a FEI Tecnai G^2 F20 with a field emission gun at a working voltage of 200 kV. All images are recorded as zero-loss images by excluding the contributions of inelastically scattered electrons using a Gatan Image Filter.

Thermal Property. The thermal degradation of the nanocomposites with different particle loadings is studied by a thermo-gravimetric analysis (TGA, TA Instruments TGA Q-500). TGA is conducted on the pure epoxy and Fe@FeO/epoxy nanocomposites from 25 to 800 °C with a nitrogen flow rate of 60 mL/min and a heating rate of 10 °C/min.

Magnetic Property. The magnetic properties of the nanocomposites at room temperature are carried out in a 9 T physical properties measurement system (PPMS) by Quantum Design.

Electrical Resistance. The volume resistivity is determined by measuring the DC resistance along the length direction of rectangular bars with dimensions of 40 × 12 × 3 mm^3. An Agilent 4339B high resistance meter is used to measure the samples. This equipment allows resistivity measurement up to 10^{16} Ω. The source voltage is adapted to the resistivity and is adjusted 100 V for pristine epoxy and nanocmopposites with 1 and 5 wt % Fe@FeO nanoparticles. The voltage is set at 10 V for nanocomposites with 10 wt % Fe@FeO nanoparticle loading and 1 V for 20 wt % Fe@FeO/epoxy nanocomposites. The resistivity is converted to volume resistivity, ρ_v, using eq 1

$$\rho_v = WDR_v/L \quad (1)$$

where W is the width, D is the thickness, L is the length of the sample, and R_v is the measured resistance. The reported values represent the mean value of 8 measurements with a deviation less than 10%.

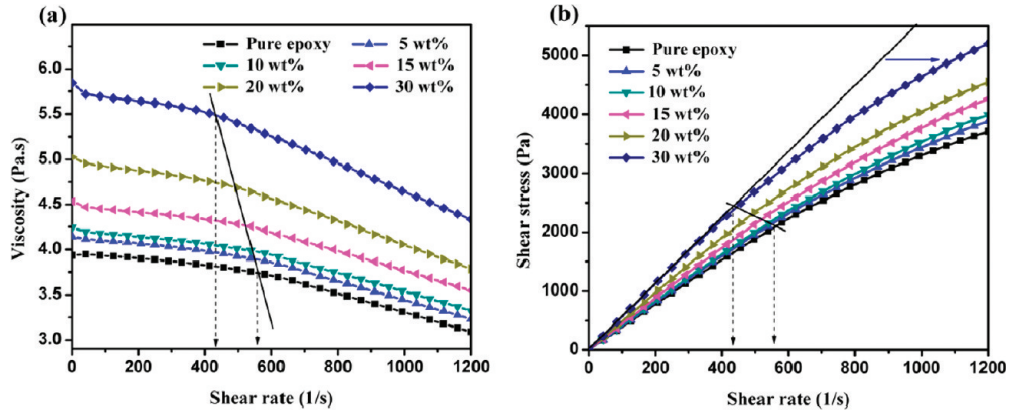

FIGURE 1. (a) Viscosity and (b) shear stress vs shear rate of pristine epoxy monomer and monomer/NPs solution system.

Table 1. Parameters in Cross Model for Pure Epoxy and Nanocomposites

	η_0 (Pa s)	η_∞ (Pa s)	C ($\times 10^{-4}$ s)	m
pure epoxy	3.932	1.279	3.751	2.274
5 wt % Fe@FeO/epoxy	4.109	1.298	3.963	2.129
10 wt % Fe@FeO/epoxy	4.192	1.047	4.189	1.943
15 wt % Fe@FeO/epoxy	4.471	0.606	4.635	1.965
20 wt % Fe@FeO/epoxy	4.955	0.410	4.737	1.936
30 wt % Fe@FeO/epoxy	5.734	1.373	5.692	1.948

RESULTS AND DISCUSSION

Rheological Property of Fe@FeO/Epoxy Monomer Resin Suspensions. Panels a and b in Figure 1 show the viscosity and shear stress as a function of shear rate for the pure epoxy monomers and nanocomposite suspensions. Both the viscosity and shear stress of nanocomposites are observed to be much higher than that of the pure epoxy. Cross' rheological model is employed (26, 27) to correlate the viscosity and shear rate, eq 2

$$\eta = \eta_\infty + \frac{\eta_0 - \eta_\infty}{1 + (C\dot{\gamma})^m} \qquad (2)$$

where η_0 is the zero shear viscosity, the magnitude of the viscosity at the lower Newtonian plateau. η_∞ is the infinite shear viscosity. C is known as the cross time constant (or consistency). The reciprocal, $1/C$, determines the critical shear rate, which is useful for evaluating the onset shear rate for shear thinning. $\dot{\gamma}$ represents the shear rate. m is the dimensionless cross rate constant, which is a measure of the degree of viscosity dependence on the shear rate in the shear-thinning region. A value of zero for m indicates Newtonian behavior with m tending to unity for increasingly shear thinning behavior. The calculated values of η_0, $\boldsymbol{\eta}_\infty$, C, and m are summarized in Table 1.

It is obvious that η_0 increases with the increase of nanoparticle loading. In addition, we found that there exists a critical shear rate ($\dot{\gamma}_c$), which is defined as the onset point of shear thinning transition. The higher the nanoparticle loading, the earlier the shear thinning transition of the nanocomposites is observed, Figure 1a. The deviation of the shear stress-shear rate curve from the straight line beginning from the critical shear rate further demonstrates the shear thinning behavior of the nanocomposites. The earlier shear thinning behavior of the nanocomposites is also revealed by the increase of C (Table 1), which increases from 3.751 $\times$ 10^{-4} s to 5.692 $\times$ 10^{-4} s as the particle loading increases from 5 to 30 wt %. Earlier shear thinning phenomenon with the increase of the particle loading is also reported in poly(ethylene oxide)/organoclay nanocomposites, which is due to the orientation of silicate layers and polymer conformation changes under shear (28). In this work, the shear thinning mainly arises from the alignment of polymer molecular chains under shear stress (29). In addition, the rolling effect of spherical nanoparticles will promote the laminar motion of the fluid, thus an earlier shear thinning is observed. A strong decrease in viscosity of polymer nanocomposites induced by sphere-shaped nanoparticle is also reported in other work (30–32). The relatively lower value of m for the nanocomposites with particle loading over 5 wt % indicates that the viscosity is less dependent on the shear rate in the shear thinning region as compared to those of the pure epoxy and 5 wt % Fe@FeO/epoxy nanocomposites.

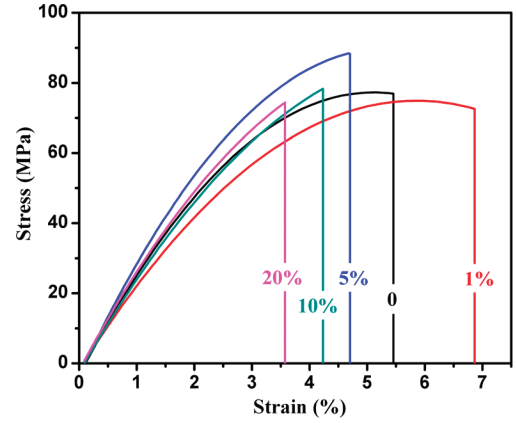

FIGURE 2. Stress–strain curve: (a) pristine epoxy, and nanocomposites with different Fe@FeO loadings of (b) 1, (c) 5, (d) 10, and (e) 20 wt %.

Tensile Property of Cured Epoxy and Its Nanocomposites. Figure 2 shows the typical tensile stress–strain curves of the cured pristine epoxy and its nanocomposites with different particle loadings. The nanocomposites filled with 1 wt % Fe@FeO nanoparticles exhibit a slightly reduced tensile strength and larger strain as

Table 2. Density and Tensile Properties of Pristine Epoxy and Nanocomposites

	composition (Fe@FeO/epoxy)				
tensile properties	pristine epoxy	1 wt %	5 wt %	10 wt %	20 wt %
density (g/cm^3)	1.194	1.196	1.220	1.287	1.391
Young's modulus (GPa)	2.39 ± 0.04	2.29 ± 0.03	2.53 ± 0.05	2.57 ± 0.03	2.64 ± 0.04
elongation-to-break (%)	5.46 ± 0.42	6.87 ± 0.37	4.80 ± 0.40	4.23 ± 0.25	3.67 ± 0.38

compared to those of the cured pristine epoxy. The elongation of the nanocomposites decreases gradually with the increase of the nanoparticle loading. As compared to the pristine epoxy, the addition of 5 wt % nanoparticles increases the tensile strength by a factor of 9.8% while sacrificing the elongation by 12%. As the particle loading further increases to 10 and 20 wt %, the tensile strength of the nanocomposites is almost the same as compared to that of the pristine epoxy, Figure 2. And the elongation decreases by 22.4 and 32.8%, respectively. It is well-known that the tensile strength of polymer nanocomposites is strongly related to the shape and content of the nanofillers. The optimal content of nanomaterials for optimal mechanical strength has been widely studied: single-walled carbon nanotube (SWNT)/nylon 6 (0.2 wt %) (33), montmorillonite/polyurethane (1 wt %) (34), and only reduced mechanical strength is obtained in poly(ε-caprolactone)/clay nanocomposites (1−10 wt %) (35). In this work, the mechanical strength is well-maintained even when the particle loading is as high as 20 wt %. This arises from the fairly uniform dispersion of nanoparticles and the strong interaction between the nanoparticles and polymer, which facilitate maintainence of the continuity of the polymer matrix and are essentially important for the fabrication of multifunctional nanocomposites with a high mechanical strength.

The variation of Young's modulus with particle loading is summarized in Table 2. The Young's modulus decreases from 2.39 GPa for the pure epoxy to 2.29 GPa for the nanocomposites with 1 wt % particle loading. While the Young's modulus increases gradually from 2.53 to 2.64 GPa for the nanocomposites with the loading increases from 5 to 20 wt %. The variation of elongation-to-break with the increase of particle loading shows opposite trend as compared to the change of Young's modulus. These results indicate the improved stiffness and reduced toughness of the nanocomposites, which are consistent with the experimental observations of the balanced stiffness/toughness in layered silicates/epoxy nanocomposites (36).

DMA Property. Figure 3 shows the dynamic mechanical analysis (DMA) curves of the epoxy nanocomposites as a function of Fe@FeO nanoparticle loading. The DMA curve provides specific information on the storage modulus (G'), loss modulus (G'') and tanδ within the temperature range investigated. The G' reflects the elastic modulus of nanocomposites, whereas G'' is related to the energy dissipation associated with the motion of polymer chain (37). Figure 3a shows the G' as a function of the temperature for the pristine epoxy and its nanocomposites with various Fe@FeO nanoparticle loadings. The G' (1.1 GPa) for the nanocomposites containing 20 wt % Fe@FeO nanoparticles exhibits 4% increment, as compared with that (1.06 GPa) of the pristine epoxy within the glassy plateau (at 60 °C) and increases by 82.4% within the rubbery plateau (at 160 °C) from 7.84 MPa to 14.30 MPa. The significant increase in G' is ascribed to the confinement and well dispersion of the nanoparticles in the matrix. Similar trend is observed for the change of G'' as the temperature increases, Figure 3b.

The tan δ is the ratio of the loss modulus to the storage modulus, and the peak of the tan δ is often used to determine the glass transition temperature (T_g). It is noteworthy that the nanocomposites undergo higher glass-transition temperatures, which is about 10 °C increase as compared to that of the cured pristine epoxy. The height of the tan δ peak decreases from 1.1 to 0.7 with the addition of nanoparticles, Figure 3c, which indicates the enhanced elastic properties of nanocomposites. Furthermore, the peak of tan δ (T_g) is significantly shifted to higher temperature for the nanocomposites as compared to the pristine epoxy. This observation is due to the strong interaction between nanoparticles and the epoxy matrix. The mechanism of the curing process around the nanoparticles is proposed in Figure 4.

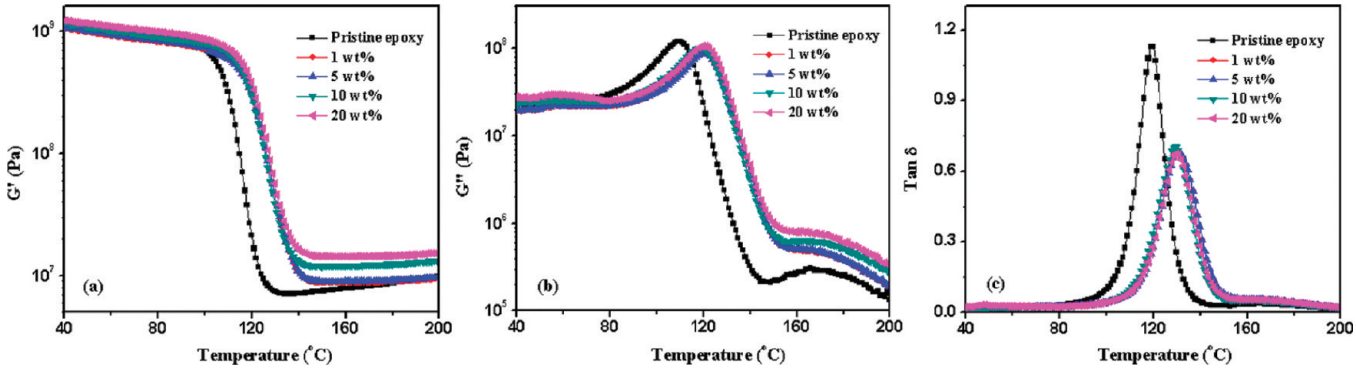

FIGURE 3. (a) Storage modulus (G'), (b) loss modulus (G''), and (c) tan δ vs temperature curves for nanocomposites with different Fe@FeO loadings, respectively.

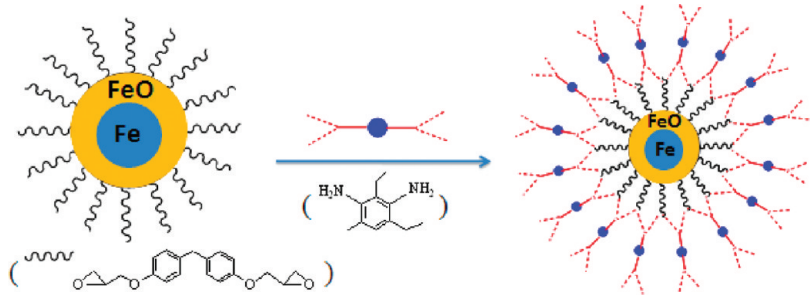

FIGURE 4. Schematic curing process on nanoparticle surface.

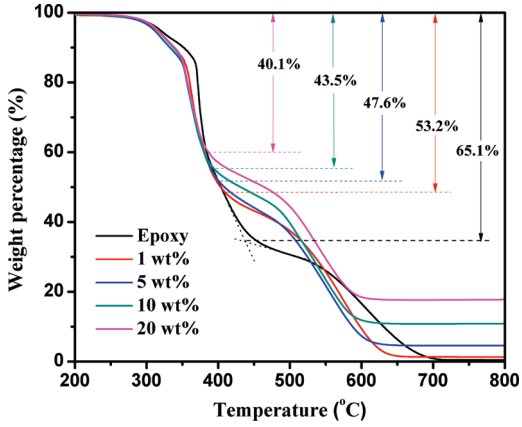

FIGURE 5. TGA curve of pristine epoxy and nanocomposites.

Table 3. TGA Results of Pristine Epoxy and Nanocomposites[a]

samples	$T_{1\ onset}$ (°C)	$T_{2\ onset}$ (°C)	$T_{5\%}$ (°C)
epoxy	364.5	549.8	319.0
1 wt % Fe@FeO/epoxy	345.4	509.6	314.7
5 wt % Fe@FeO/epoxy	338.9	500.8	314.6
10 wt % Fe@FeO/epoxy	339.1	499.1	315.5
20 wt % Fe@FeO/epoxy	338.0	497.9	315.7

[a] $T_{1\ onset}$ and $T_{2\ onset}$ indicate the onset degradation temperature of first and second stage, respectively. $T_{5\%}$ represents the temperature of degradation at which the weight loss is 5%.

The nanoparticles are completely wetted by epoxy monomers and then cross-linking between monomers on particle surface and curing agent in bulk solution is performed during curing process. T_g of a polymer is known to depend on the mobility of the chain segment of the macromolecules in the polymer matrix. In this case, the nanoreinforcement of the nanoparticles in polymer matrix restricts the motion of macromolecule chains and thus increases the glass-transition temperatures of nanocomposites.

Thermalgravimetric Analysis. Figure 5 shows the thermalgravimetric analysis (TGA) curves of the pristine epoxy and its nanocomposites. Both pristine epoxy and nanocomposites are observed to have similar decomposition profiles and the degradation takes place in two stages. The first (T_{d1}) and second (T_{d2}) onset decomposition temperature, as well as the 5% weight loss temperature ($T_{5\%}$) are summarized in Table 3. The thermal stability of the nanocomposites is observed to slightly decrease as compared to that of the pristine epoxy. With the addition of the nanoparticles, the T_{d1}, T_{d2}, and $T_{5\%}$ of the nanocomposites are decreased by about 20, 50, and 5 °C, respectively. This may result from the spatial obstruction of nanoparticles on the formation of high cross-linked molecular structure of epoxy or increased free volume fractions in the polymer nanocomposites (38, 39). It is interesting to find that the T_{d1}, T_{d2}, and $T_{5\%}$ are less dependent on the proportion of nanoparticles in the nanocomposites, especially when the loading exceeds 5 wt %. The difference of T_{d1} and T_{d2} for nanocomposites with different loadings is less than 10 °C, and even less for $T_{5\%}$. Although the thermal stability of the nanocomposites decreases to some extent after the incorporation of nanoparticles, the slight deleteriousness of thermal stability with higher particle loading gives us some essential guidance to designing nanocomposites that are required for high particle loadings to obtain improved physical properties, such as magnetic, electric, and microwave absorption properties (10, 40). The total weight loss of the first degradation stage is shown in Figure 5 (marked with arrows), which decreases gradually with the increase in the particle loadings and is attributed to the restriction of the nanoparticles on the long-range chain mobility of the epoxy phase within the nanocomposites.

SEM Investigation on the Fracture Surface. The microstructure of the fracture surfaces of both pristine epoxy and nanocomposites with different loadings is shown in Figure 6. The cured pristine epoxy shows a smooth fracture surface while the PNCs show a rough fracture surface, Figure 6a–c. The rough surface is attributed to the matrix shear yielding or the polymer deformation between the nanoparticles (41). The enlarged SEM image of the pristine epoxy, Figure 6d, exhibits banded deformation and the cracked polymer flakes are clearly observed on the fracture surface. However, no flakes are observed on the fracture surface after the addition of the nanoparticles, which indicates a strong bonding between the nanoparticles and the epoxy matrix. Moreover, the nanoparticles are well embedded in the epoxy matrix and no interfacial voids are observed even at high particle loading of 20 wt % (Figure 6e,f), which indicates that the tensile fracture deformation occurs between the polymer chains rather than from the nanoparticle–polymer interface. All these observations are in good agreement with the results of the tensile properties of nanocomposites.

Magnetic Property and Particle Distribution Investigation. Figure 7A shows the magnetic hysteresis loops of the as-received Fe@FeO nanoparticles and Fe@FeO/epoxy nanocomposites with a 20 wt % nanoparticle loading. The saturation magnetization (M_s) is evaluated at the state when an increase in magnetic field can not increase the

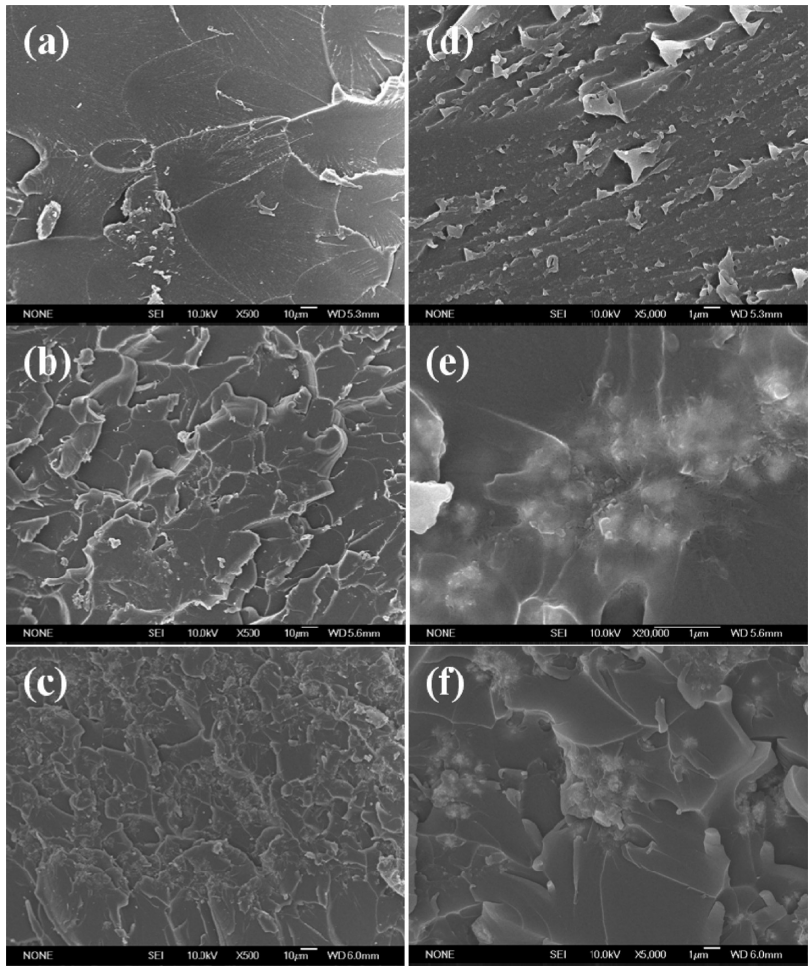

FIGURE 6. SEM micrographs of (a) the pristine epoxy, and the nanocomposites filled with (b) 5 and (c) 20 wt % Fe@FeO NPs. (d−f)Enlarged fracture surface of a−c, respectively.

magnetization of the material further. Magnetization is observed to reach saturated at high magnetic field for both Fe@FeO nanoparticles (108.07 emu/g) and Fe@FeO/epoxy nanocomposites (17.05 emu/g), Figure 7A. The field required to saturate is much lower after the nanoparticles are dispersed in the polymer matrix. The coercivity (H_c, Oe) indicates the external applied magnetic field required to return the material to zero magnetization condition and the remnant magnetization (M_r) is the residue magnetization after the applied field is reduced to zero. Both values are read from the axes crossover points, which are clearly shown in Figure 7A (inset figures). The coercivity increases from 62.33 Oe for Fe@FeO nanoparticles to 202.13 Oe after the nanoparticles are dispersed in the epoxy matrix. This indicates that the Fe@FeO nanoparticles become magnetically harder after dispersing in epoxy. The enhanced coercivity of nanocomposites is due to the decreased interparticle dipolar interaction, which arises from the enlarged nanoparticle spacer distance for the single domain nanoparticles (16, 19, 42), as compared to the closer contact of the pure nanoparticles. Figure 7B shows the TEM images of PNCs with a loading of 5 and 20 wt %, respectively. Partial particle agglomeration is observed in both the SEM and low-magnification TEM images in some areas. However, in nanoscale, the particles are well-separated and dispersed fairly uniformly in the epoxy matrix, Figure 7B-b,d, indicating a good dispersion, which is related to the free-path of the particles (43, 44). Intimate contact between the nanoparticles and the polymer is observed without any interfacial voids observed from the high-magnification TEM observations. This result demonstrates the feasibility of this simple surface wetting method to prevent the nanoparticle agglomeration at the nanoscale. Moreover, the increased interparticle distance is well-consistent with the enhancement of the coercivity in the nanocomposites as compared to the contacted pure nanoparticles. The inset of Figure 7B-a gives the core−shell structure of the nanoparticles.

Electrical Conductivity. Figure 8 shows the volume resistivity of epoxy nanocomposites filled with different loadings of Fe@FeO nanoparticles. The resistivity decreases slightly when the particle loading increases from 1 to 5 wt %. A further decrease in resistivity of 5−6 orders of magnitude appears by increasing the nanoparticle loading from 5 to 10 wt %. However, the resistivity does not change a lot when the loading is above 10 wt %, only a slight decrease of less than 1 order of magnitude is observed. These significant changes in resistivity indicate that an infinite network structure of the percolated Fe@FeO nanoparticles begins to form around 10 wt % (about 1.5 vol %). In the

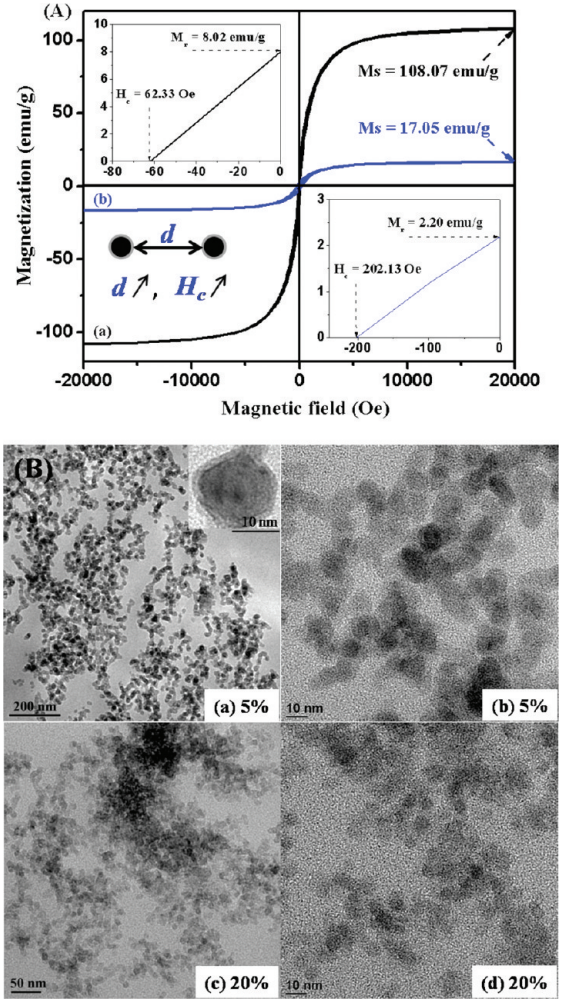

FIGURE 7. (A) Hysteresis loops of (a) Fe@FeO nanoparticles and (b) 20 wt % Fe@FeO/epoxy nanocomposites at room temperature. (B) TEM images of the nanocomposites with particle loadings of (a, b) 5 wt % and (c, d) 20 wt % with different magnifications.

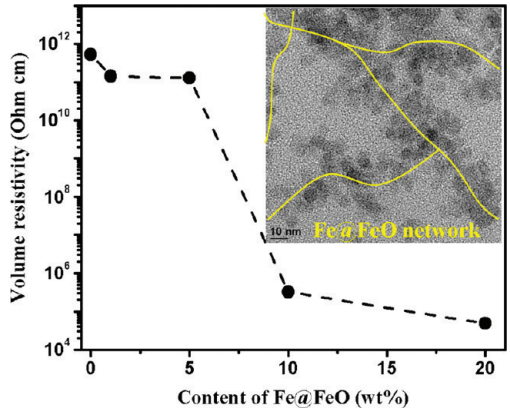

FIGURE 8. Effect of Fe@FeO content on volume resistivity of nanocomposites.

most prominent geometrical models created by Kirkpatrick (45) and Zallen (46), the required minimum touching spherical particles is 16 vol %. This value is in approximately agreement with most experimental observations that the critical volume fraction is between 5 and 20 vol % for PNCs filled with powdery materials. However, this model can not explain the experimentally observed percolation threshold that the PNCs exhibits significantly enhanced conductivity at the loading of 1.5 vol %. The systematic studies on carbon black nanoparticles dispersed in the epoxy resin reveal that the percolation threshold not only depends on the particle size and fractal dimension, but also depends on shear rate used to dispersion carbon black (47). Using this approach, the percolation can be achieved as low as 0.3 vol %. Even lower electrical percolation (<0.1 wt %) was found in PNCs filled with carbon nanotubes owning to the large aspect ratio (48−50). The relatively low percolation as determined in this work is arising from the network structure constructed by the submicrometer nanoparticle aggregates with uniformly dispersed particles in nanoscale, as evidenced by the SEM and TEM investigations (Figure 7B). However, the density increases about 16 wt % for the nanocomposites with a particle loading of 20 wt %, Table 2.

CONCLUSIONS

Conductive epoxy resin nanocomposites with superior magnetic properties are prepared by dispersing core−shell structured Fe@FeO nanoparticles in epoxy matrix. The viscosity of the Fe@FeO/epoxy monomer nanocomposite solutions with various particle loadings is well correlated to the Cross' rheological model. The mechanical and thermal properties of the cured nanocomposites show less dependence on the nanoparticle loadings, which is essentially important for applications obtaining strong optical, electrical, and magnetic properties. With the particle loading is varied from 1 to 20 wt %, the DMA results show the same enhancement of 10 °C in glass transition temperature for each sample. The tensile strength of the nanocomposites is well maintained even at high particle loadings. Though the thermal stability of the nanocomposites is slightly decreased as compared to the pristine epoxy, similar degradation temperatures are still observed at different loadings. The saturation magnetization (M_s) increases with the increase of particle loading. M_s is 17.03 emu/g for the epoxy nanocomposites with a Fe@FeO particle loading of 20 wt %, which is 15.8% of that of the pure nanoparticles. Meanwhile, the coercivity (H_c) increases from 62.33 to 202.13 Oe after the nanoparticles are dispersed in the epoxy resin matrix. TEM observation reveals a network structure of the nanoparticles. The higher the particle loading, the lower the electrical resistance observed. The particle percolation is found to be around 5−10 wt %, where the resistance of the nanocomposites sharply decreases by 6 orders of magnitude.

Acknowledgment. This work is supported by the research start-up fund from Lamar University. The financial supports from Dan F. Smith Department of Chemical Engineering and College of Engineering at Lamar University for obtaining the TA Rheometer are kindly acknowledged.

REFERENCES AND NOTES

(1) Guo, Z.; Henry, L. L.; Palshin, V.; Podlaha, E. J. *J. Mater. Chem.* **2006**, *16*, 1772–1777.
(2) Castro, C.; Ramos, J.; Millan, A.; Gonzalez, C.; Palacio, F. *Chem. Mater.* **2000**, *12*, 3681–3688.
(3) Yong, V.; Hahn, H. T. *Nanotechnology* **2004**, *15*, 1338–1343.
(4) Mack, J. J.; Viculis, L. M.; Ali, A.; Luoh, R.; Yang, G.; Hahn, H. T.; Ko, F. K.; Kaner, R. B. *Adv. Mater.* **2005**, *17*, 77–80.

(5) Sandi, G.; Joachin, H.; Kizilel., R.; Seifert, S.; Carrado, K. A. *Chem. Mater.* **2003**, *15*, 838–843.
(6) Zhu, J.; Wei, S.; Chen, X.; Karki, A. B.; Rutman, D.; Young, D. P.; Guo, Z. *J. Phys. Chem. C* **2010**, *114*, 8844–8850.
(7) Zhu, J.; Wei, S.; Ryu, J.; Budhathoki, M.; Liang, G.; Guo, Z. *J. Mater. Chem.* **2010**, *20*, 4937–4948.
(8) Chang, H. Y.; Lin, C. W. *J. Membr. Sci.* **2003**, *218*, 295–306.
(9) Phang, S. W.; Tadokoro, M.; Watanabe, J.; Kuramoto, N. *Synth. Met.* **2008**, *158*, 251–258.
(10) Guo, Z.; Lee, S. E.; Kim, H.; Park, S.; Hahn, H. T.; Karki, A. B.; Young, D. P. *Acta Mater.* **2009**, *57*, 267–277.
(11) Tang, T.; Chen, X.; Chen, H.; Meng, X.; Jiang, Z.; Bi, W. *Chem. Mater.* **2005**, *17*, 2799–2802.
(12) Zanetti, M.; Camino, G.; Canavese, D.; Morgan, A. B.; Lamelas, F. J.; Wilkie, C. A. *Chem. Mater.* **2002**, *14*, 189–193.
(13) Shimada, T.; Ookubo, K.; Komuro, N.; Shimizu, T.; Uehara, N. *Langmuir* **2007**, *23*, 11225–11232.
(14) Li, J.; Claude, J.; Norena-Franco, L. E.; Seok, S. I.; Wang, Q. *Chem. Mater.* **2008**, *20*, 6304–6306.
(15) An-Hui, L.; Salabas, E. L.; Ferdi, S. *Angew. Chem., Int. Ed.* **2007**, *46*, 1222–1244.
(16) Guo, Z.; Lei, K.; Li, Y.; Ng, H. W.; Prikhodko, S.; Hahn, H. T. *Compos. Sci. Technol.* **2008**, *68*, 1513–1520.
(17) Gyergyek, S.; Huskic, M.; Makovec, D.; Drofenik, M. *Colloids Surf., A* **2008**, *317*, 49–55.
(18) Baker, C.; Ismat Shah, S.; Hasanain, S. K. *J. Magn. Magn. Mater.* **2004**, *280*, 412–418.
(19) Guo, Z.; Lin, H.; Karki, A. B.; Wei, S.; Young, D. P.; Park, S.; Willis, J.; Hahn, T. H. *Compos. Sci. Technol.* **2008**, *68*, 2551–2556.
(20) Guo, Z.; Wei, S.; Shedd, B.; Scaffaro, R.; Pereira, T.; Hahn, H. T. *J. Mater. Chem.* **2007**, *17*, 806–813.
(21) Xu, Z.; Hou, Y.; Sun, S. *J. Am. Chem. Soc.* **2007**, *129*, 8698–8699.
(22) Chun-Shan, W.; Jeng-Yueh., S. *J. Appl. Polym. Sci.* **1999**, *73*, 353–361.
(23) Hergenrother, P. M.; Thompson, C. M.; Smith, J. J. G.; Connell, J. W.; Hinkley, J. A.; Lyon, R. E.; Moulton, R. *Polymer* **2005**, *46*, 5012–5024.
(24) Allaoui, A.; Bai, S.; Cheng, H. M.; Bai, J. B. *Compos. Sci. Technol.* **2002**, *62*, 1993–1998.
(25) Kuang-Ting, H.; Justin, A.; Suresh, G. A. *Nanotechnology* **2003**, *14*, 791–793.
(26) Abdullah, M. K.; Abdullah, M. Z.; Mujeebu, M. A.; Kamaruddin, S.; Ariff, Z. M. *J. Reinf. Plast. Compos.* **2009**, *28*, 2527–2538.
(27) Line-Hwa, C.; Wen-Yen, C.; Chao-Hsun, C.; Hsieng-Cheng, T. *J. Appl. Polym. Sci.* **1999**, *71*, 39–46.
(28) Hyun, Y. H.; Lim, S. T.; Choi, H. J.; Jhon, M. S. *Macromolecules* **2001**, *34*, 8084–8093.
(29) Chen, Z. R.; Issaian, A. M.; Kornfield, J. A.; Smith, S. D.; Grothaus, J. T.; Satkowski, M. M. *Macromolecules* **1997**, *30*, 7096–7114.
(30) Tuteja, A.; Duxbury, P. M.; Mackay, M. E. *Macromolecules* **2007**, *40*, 9427–9434.
(31) Mackay, M. E.; Tuteja, A.; Duxbury, P. M.; Hawker, C. J.; Van Horn, B.; Guan, Z.; Chen, G.; Krishnan, R. S. *Science* **2006**, *311*, 1740–1743.
(32) Mackay, M. E.; Dao, T. T.; Tuteja, A.; Ho, D. L.; Van Horn, B.; Kim, H.-C.; Hawker, C. J. *Nat. Mater.* **2003**, *2*, 762–766.
(33) Gao, J.; Itkis, M. E.; Yu, A.; Bekyarova, E.; Zhao, B.; Haddon, R. C. *J. Am. Chem. Soc.* **2005**, *127*, 3847–3854.
(34) Tien, Y. I.; Wei, K. H. *Polymer* **2001**, *42*, 3213–3221.
(35) Lepoittevin, B.; Devalckenaere, M.; Pantoustier, N.; Alexandre, M.; Kubies, D.; Calberg, C.; Jérôme, R.; Dubois, P. *Polymer* **2002**, *43*, 4017–4023.
(36) Carsten, Z.; Rolf, M.; Jügen, F. *Macromol. Chem. Phys.* **1999**, *200*, 661–670.
(37) Hsueh, H. B.; Chen, C. Y. *Polymer* **2003**, *44*, 5275–5283.
(38) Pan, Y.; Xu, Y.; An, L.; Lu, H.; Yang, Y.; Chen, W.; Nutt, S. *Macromolecules* **2008**, *41*, 9245–9258.
(39) Shi, Y.; Peterson, S.; Sogah, D. Y. *Chem. Mater.* **2007**, *19*, 1552–1564.
(40) Guo, Z.; Park, S.; Wei, S.; Pereira, T.; Moldovan, M.; Karki, A. B.; Young, D. P.; Hahn, H. T. *Nanotechnology* **2007**, *18*, 335704/1–8.
(41) Guo, Z.; Pereira, T.; Choi, O.; Wang, Y.; Hahn, H. T. *J. Mater. Chem.* **2006**, *16*, 2800–2808.
(42) Zhang, D.; Karki, A. B.; Rutman, D.; Young, D. P.; Wang, A.; Cocke, D.; Ho, T. H.; Guo, Z. *Polymer* **2009**, *50*, 4189–4198.
(43) Luo, Z.; Koo, J. H. *J. Microsc.* **2007**, *225*, 118–125.
(44) Luo, Z. *J. Mater. Sci.* **2010**, *45*, 3228–3241.
(45) Kirkpatrick, S. *Rev. Mod. Phys.* **1973**, *45*, 574–588.
(46) Zallen, R. *The Physics of Amorphous Solids*; Wiley: New York, 1983.
(47) Ruediger, S.; Juergen, P.; Karl, S.; Hans-Peter, W. *J. Appl. Polym. Sci.* **1997**, *63*, 1741–1746.
(48) Thostenson, E. T.; Chou, T. W. *Carbon* **2006**, *44*, 3022–3029.
(49) Sandler, J. K. W.; Kirk, J. E.; Kinloch, I. A.; Shaffer, M. S. P.; Windle, A. H. *Polymer* **2003**, *44*, 5893–5899.
(50) Thostenson, E. T.; Ziaee, S.; Chou, T. W. *Compos. Sci. Technol.* **2009**, *69*, 801–804.

AM100361H